Neuronal Correlates of Kinematics-to-Dynamics Transformation in the Supplementary Motor Area

Camillo Padoa-Schioppa,[1,2] Chiang-Shan Ray Li,[3]
and Emilio Bizzi
McGovern Institute for Brain Research
Department of Brain and Cognitive Sciences
Massachusetts Institute of Technology
Cambridge, Massachusetts 02139

Summary

It is widely acknowledged that movements are planned at the level of the kinematics. However, the central nervous system must ultimately transform kinematic plans into dynamics-related commands. How, when, and where the kinematics-to-dynamics (KD) transformation is processed represent fundamental and unanswered questions. We recorded from the supplementary motor area (SMA) of two monkeys as they executed visually instructed reaching movements. We specifically analyzed a delay period following the instruction but prior to the go signal (motor planning). During the delay, a group of neurons in the SMA progressively came to reflect the dynamics rather than the desired kinematics of the upcoming movement. This finding suggests that some neurons in the SMA participate in the KD transformation.

Introduction

Reaching movements can be described at two different levels: kinematics and dynamics. The term kinematics refers to the evolution in time of the joint angles and hand position. The term dynamics refers to the set of forces exerted by the muscles. In Newtonian mechanics, the causal relationship flows from dynamics to kinematics, that is, muscle forces cause hand movements. The central nervous system, however, is faced with the inverse problem: given a desired hand trajectory (the desired kinematics), how to generate appropriate muscle forces (the dynamics). Thus, a central problem in motor control is that of transforming desired kinematics into suitable dynamics (Alexander and Crutcher, 1990a; Kalaska and Crammond, 1992; Mussa-Ivaldi and Bizzi, 2000; Saltzman, 1979).

From a computational perspective, the processing of the (inverse) dynamics presents a difficult challenge, which the central nervous system (CNS) may deal with by using forward internal models (Shadmehr and Mussa-Ivaldi, 1994; Kawato, 1999; Wolpert and Ghahramani, 2000). In essence, internal models for the dynamics describe the dynamic properties of the limb and the environment. Previous work in humans and monkeys has found that new internal models can be acquired through

experience (Shadmehr and Mussa-Ivaldi, 1994; Li et al., 2001). When subjects adapt to perturbing forces, they learn to transform the same desired kinematics into new dynamics appropriate for the novel dynamic environment (Shadmehr and Mussa-Ivaldi, 1994; Wolpert and Ghahramani, 2000; Bhushan and Shadmehr, 1999). In addition, it was found that internal models for the dynamics are acquired independently of internal models for the kinematics, which subjects learn when the association between the visual stimulus and the instructed movement is perturbed (Krakauer et al., 1999; Flanagan et al., 1999). Internal models for both the kinematics and the dynamics undergo consolidation in the hours following acquisition.

It has been suggested that the neuronal representation of the internal models for the movement dynamics may be partly stored in the cerebellum (Shidara et al., 1993; Imamizu et al., 2000). However, processing of the dynamics occurs across multiple cortical and subcortical areas. Numerous studies in monkeys have investigated the dynamics-related activity of single neurons in different motor areas by comparing the activity recorded in the absence of perturbation with that recorded in the presence of perturbing forces (or loads) to which the monkeys had adapted. These studies have found dynamics-related neuronal activity during motor execution in the primary motor cortex (M1; Evarts, 1968; Kalaska et al., 1989; Crutcher and Alexander, 1990; Li et al., 2001), the supplementary motor area (SMA; Crutcher and Alexander, 1990), the dorsal premotor area (PMd; Werner et al., 1991), the ventral premotor area (PMv; Hepp-Reymond et al., 1994), the putamen (Crutcher and Alexander, 1990), and the dentate and interpositus nuclei of the cerebellum (Thach, 1978). In contrast, no dynamics-related activity was found in area 5 (Kalaska et al., 1990).

Some of the motor areas displaying dynamics-related activity during motor execution, such as the SMA and the PMd, also show prominent activation during motor planning (Alexander and Crutcher, 1990a; Tanji, 1994; Kurata and Wise, 1988; Wise et al., 1997). With the intent of investigating the neuronal correlates of the kinematics-to-dynamics (KD) transformation, we studied dynamics-related activity during motor planning. In particular, we recorded the activity of neurons in the SMA (also called SMA-proper or F3). This area (as distinguished from the adjacent and more rostral preSMA) is densely interconnected with the primary motor cortex and with other premotor areas of the frontal lobe and sends direct anatomical projections to the spinal cord (He et al., 1995; Matelli et al., 1991; Luppino et al., 1991). Recent studies implicate the SMA in more "concrete aspects of movement" (Picard and Strick, 2001) than previously thought (Matsuzaka et al., 1992; Hikosaka et al., 2000; Picard and Strick, 1996).

Consistent with previous reports (Alexander and Crutcher, 1990a), we found neurons in the SMA whose activity during motor planning reflects the dynamics of the upcoming movement. We confirmed this finding with a population analysis. In addition, we found that some

[1] Correspondence: camillo@alum.mit.edu
[2] Present address: Department of Neurobiology, Harvard Medical School, WAB 224, 200 Longwood Avenue, Boston, MA 02115.
[3] Present address: Psychiatry Service 116A, Building 1, 9th Floor, East Wing, Yale University/VA Medical Center, West Haven, CT 06516.

neurons in the SMA come to reflect the movement dynamics increasingly during the phase of motor planning, starting from a kinematics-related signal. This observation suggests that the activity of these neurons reflects the KD transformation. Two measures of correlation between the dynamics-related neuronal activity and the performance in the task support this interpretation. We conclude (1) that the movement dynamics may be partly processed during motor planning and long before the initiation of the movement, and (2) that neurons in the SMA may participate, together with neurons in other areas, in the neuronal processing of the KD transformation.

Results

We used two monkeys in our experiments. During experimental sessions, one monkey held the handle of a robotic arm and executed reaching movements, instructed by targets appearing on a computer monitor. A cursor on the monitor indicated the position of the monkey's hand at any given time. To study the neuronal activity related to motor planning, we introduced a delay of variable duration (0.5–1.5 s) between the presentation of the instruction (the cue signal) and the go signal (Figure 1A). Unless otherwise specified, the present results refer to the activity prior to the go signal.

Two motors attached at the base of the robot were designed to exert forces upon the hand of the monkeys. These forces are described by force fields $F = BV$, where V is the instantaneous hand velocity and B is a rotation matrix $B = [0 - b; b \; 0]$. Depending on the sign of b, F was clockwise (CK) or counterclockwise (CCK). In each session, the monkey performed in a baseline condition (circa 160 successful trials, no forces), followed by a force condition (circa 160 successful trials) (Figure 1B).

Psychophysics

In the baseline condition, the hand trajectories were essentially straight. In the force condition, the hand trajectories were initially deviated by the perturbing force. Over trials, however, the monkeys gradually adapted to the perturbation, and the hand trajectories became straight again (Figure 1C). To quantify this adaptation process, we computed for each trial the deviation of the actual trajectory from the straight line passing through the initial position and the end point. Focusing on the initial part of the movement, we computed a weighted average of the hand position during the trajectory (exponentially decaying weights), and we transformed the resulting movement position into the corresponding angle of initial deviation d (with $d > 0$ for deviations in direction of the external force). Thus, for each trial in the force condition, d quantified the initial error. In the baseline condition, d showed some variability but averaged close to zero over trials. In the force condition, d was consistently above zero at first and gradually dropped as the monkeys adapted (Figure 1D). Thus, the actual kinematics in the force condition converged over trials to that recorded in baseline. After computing for each session the mean initial deviation ($\Delta\bar{d}$) across trials, we observed that this convergence continued over sessions (Figure

1E). The analysis of the speed profile provided very similar results (data not shown).

The fact that the actual kinematics in the force condition converged to that recorded in the baseline suggested the presence of an unaltered kinematic plan, which the monkeys gradually learned to implement by activating the muscles properly (see also Shadmehr and Mussa-Ivaldi, 1994; Li et al., 2001). In other words, in the force condition the monkeys learned to transform the same desired kinematics into a new dynamics (Figure 1F). In the following analysis, we compared the neuronal activity across the two conditions (baseline and force), disregarding the initial adaptation phase: for each condition, we excluded the first four successful trials in each movement direction.

Dynamics-Related Activity during Motor Planning

We recorded a total of 252 neurons in the forelimb region of the SMA (Figure 2). Considering the 0.3 s after the cue signal, the activity of 22 cells (9%) was directionally tuned in both the baseline and force conditions. The corresponding numbers were 81 cells (32%) for the delay time (0.5 s prior to the go signal), and 128 cells (51%) for the movement time (from 0.2 s prior to the movement onset to the movement end). In total, 153 cells (61%) were directionally tuned in at least one of the three above time windows.

To analyze the activity related to motor planning, we aligned all the trials at the go signal, and we defined the delay time (or DT time window) as the 0.5 s prior to the go signal. Figure 3A illustrates the activity of a representative cell recorded in SMA with a CK force field. The cell is represented by a tuning curve, plotted in blue in polar coordinates. The preferred direction (Pd, in red) indicates the direction for which the cell activity would optimally contribute to the movement. The DT activity of the cell is very different in the two conditions. In the baseline condition, the Pd of the cell is oriented toward 153°. In the force condition, however, the tuning curve changes and the Pd rotates CK by 36°. These changes indicate that the DT activity of the cell reflects some aspect of the dynamics of the upcoming movement. Note that the visual instructions were identical in the two conditions. Likewise, the psychophysics suggests that the desired kinematics were the same in the two conditions. Thus, the processing of the visual stimuli (Andersen et al., 1993; Newsome, 1997; Gold and Shadlen, 2000) or the processing of the desired kinematics (Wise et al., 1992; Shen and Alexander, 1997; Alexander and Crutcher, 1990b) cannot alone explain changes of neuronal activity across conditions. In addition, because the force field was proportional to the velocity ($F = BV$), no force was actually present during the delay (because $V = 0$). Thus, changes of neuronal activity do not reflect online motor execution or changes in proprioceptive feedback. Instead, the changes observed in the force condition suggest that during motor planning, the activity of the cell shown in Figure 3A reflects the dynamics of the upcoming movement.

New Dynamics and Shift of Pd in the Delay Time (DT)

In the force condition, the Pd of the cell shown in Figure 3A shifted in the direction of the external force, namely
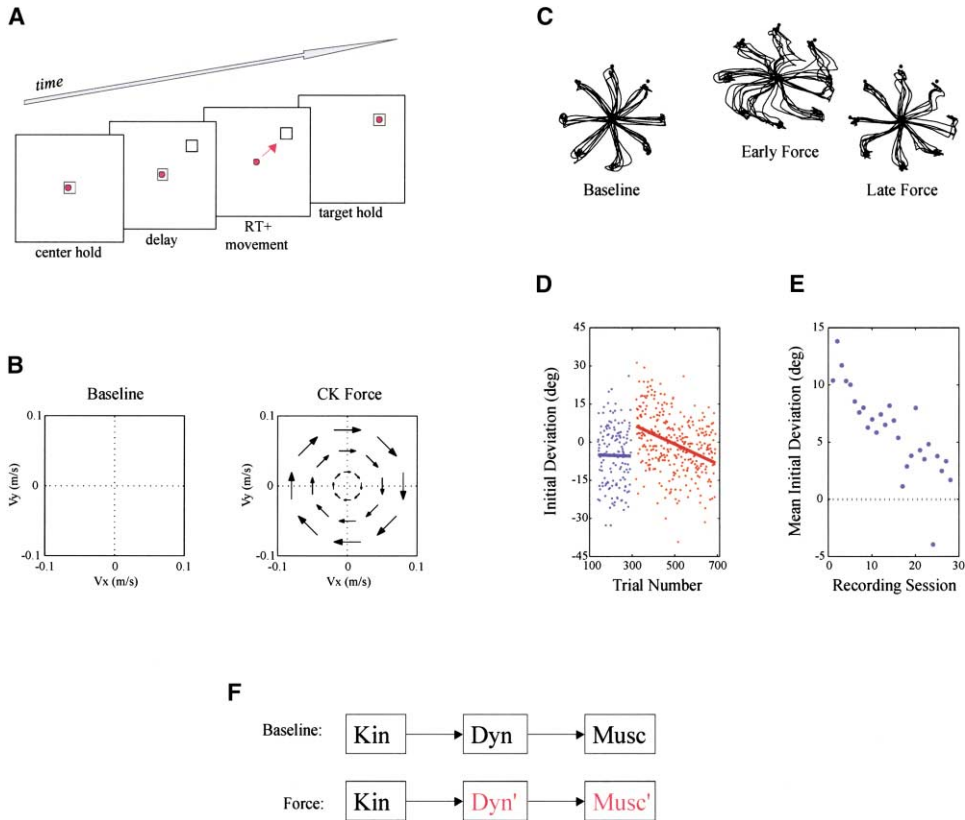
Figure 1. Experimental Design and Psychophysics

(A) Trial sequence (see Experimental Procedures for details).

(B) Experimental paradigm. There is no perturbation in the baseline condition, and there is a force field (either CK or CCK) in the force condition. The CK force field is plotted here in velocity space.

(C) Representative hand trajectories. In the baseline condition (left), the trajectories are essentially straight. When a CK force field is introduced (center, early force), the trajectories are initially deviated by the perturbing force. As the monkey adapts to the perturbation, however, the trajectories become straight again (right, late force).

(D) Initial deviation, one session. To quantify the actual kinematics, we computed the initial deviation (d) of the actual hand trajectory from the ideal straight line passing through the initial position and the end point. Here, the deviation is plotted on the y axis against the trial number (x axis) for one representative session. The deviation d is expressed in degrees and defined so that positive values of d correspond to deviations in the direction of the external force (i.e., undercompensated movements). Each trial is represented by one dot, and the solid lines are the result of a linear fit. In the baseline condition (blue), d remains essentially constant and close to zero throughout the trials. In the force condition (red), the trajectories are initially deviated ($d > 0$) and return to straight as the monkey adapts (negative slope of the linear fit). In other words, the actual kinematics recorded in the force condition gradually converge to that recorded in the baseline, indicating that the desired kinematics remain unchanged.

(E) Initial deviation, all sessions. This convergence continued over sessions. For each session, we computed the difference between the average deviation in the force condition (y average of red dots in [D]) and that in baseline (y average of blue dots in [D]). The resulting mean initial deviation $\Delta \bar{d}$ is plotted here (y axis) against the session number (x axis). All the sessions where monkey C was presented with a CCK force field are shown. The mean initial deviation, at first relatively high, gradually vanished over sessions (long-term learning).

(F) Experimental paradigm. The psychophysics of the task can be summarized as follows. In the baseline condition, the monkeys transform a desired kinematics into the corresponding dynamics. In the force condition, the monkeys learn to transform the same desired kinematics into a new dynamics. Thus, activity that changes across conditions is associated with the movement dynamics. Activity that remains unchanged is associated with the desired kinematics.

the CK direction. This was not an isolated case. We computed the Pd of all the cells that were directionally tuned in both the baseline and force conditions. A total of 81 cells satisfied this criterion and were considered for subsequent analysis. For each cell, we computed the shift of Pd in the force condition compared to baseline. The shift of Pd was defined to be greater than zero if the Pd rotated in the direction of the external force. We then performed a population analysis of the 81 neurons during the delay time. We found that the Pd of the SMA neurons shifted significantly in the force condition in the

direction of the external force (mean shift 11.1°, $p < 0.02$, circular t test; Figure 3B). Most importantly, the shift of Pd observed for the SMA cells during the delay corresponded to an analogous shift of Pd observed for muscles during the following movement. In separate sessions, we recorded the electromyographic (EMG) activity of five muscles of the upper arm (pectoralis, deltoid, biceps, triceps, and brachioradialis). We analyzed the activity of these muscles during the movement-related time window, and we found that in the force condition the Pd of muscles shifted significantly in the

A

Legend: ◆ Face △ Upper trunk ○ Forelimb + Tail □ Hindlimb
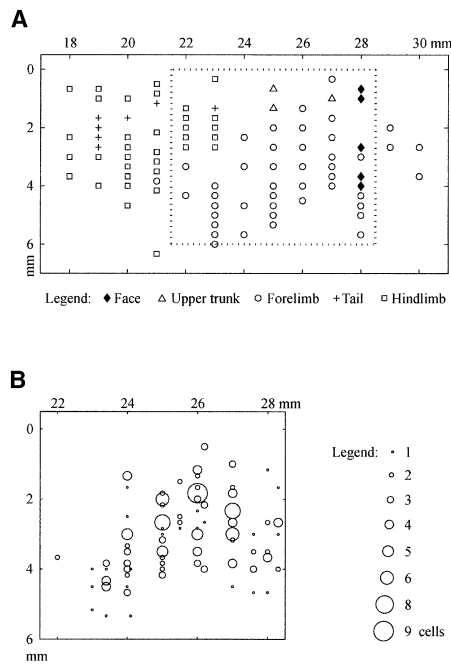
B

Legend: · 1
○ 2
○ 3
○ 4
○ 5
○ 6
○ 8
○ 9 cells

Figure 2. Microstimulation and Recordings

(A) Microstimulation of the left medial wall of monkey C. The axes indicate stereotaxic coordinates (x axis caudal to rostral, y axis dorsal to ventral), and symbols indicate body parts (see legend). Our goal was to distinguish the SMA from the neighboring areas and to identify the forelimb region within the SMA. Thus, we did not vary the current systematically and typically injected trains of 40 μA. A location was assigned when we could elicit consistent movements of one body part. For the medial wall, we closely replicated the results of Luppino et al. (1991). Caudally, the tail region marked the border between M1 and SMA. Rostrally, the face region marked the border between SMA and preSMA. In M1, we could easily elicit movements with low currents (10 μA). In contrast, we often failed to elicit any response when stimulating the preSMA. (In a few cases, we succeeded with higher currents >40 μA.) In some instances when stimulation of the preSMA was successful, we observed more complex movements (i.e., slow, multijoint movements that appeared goal directed) than those typically elicited from M1 or SMA. In the same animal, we also performed extensive microstimulation of the cingulate gyrus. The emerging map (data not shown) was congruent with maps of He et al. (1995), which were based on corticospinal projections. Within the SMA, microstimulation revealed a clear topographic organization. The cells described here were exclusively recorded in the forelimb area (dotted line) of the SMA. Recordings were confined to the medial wall (no white matter was encountered during penetrations), with lateral coordinates ranging between L(−1.5) and L(−3.5). A handful of cells were recorded from the border with the cingulate motor areas (which we located at the intersection between the medial wall and the dorsal bank of the cingulate sulcus).
(B) Location of recordings. The radius of each circle is proportional to the number of cells recorded in the corresponding location, and the cells recorded from monkey C are shown. In a separate analysis, we considered only the cells with a directionally tuned DT activity (data not shown). In essence, the distribution of locations for these cells appeared a fair down-sample of the distribution shown here. In other words, the cells with significant DT activity were randomly distributed across the region spanned during the recordings. Analysis of the mediolateral coordinate provided a similar result.

direction of the external force (mean shift 19.2°, p < 0.003, t test) (Figure 4). For muscles, the shift of Pd is imposed by the curl force fields (Thoroughman and

Shadmehr, 1999; Li et al., 2001). For cells, we regard the shift of Pd as a fingerprint of the new dynamics.

As shown in Figure 3B, neurons in the SMA display a collective shift of Pd in the force condition in the direction of the external force. This collective shift indicates that information on the dynamics of the upcoming movement is present at the level of the SMA population during motor planning. However, not all the neurons in the SMA reflect the movement dynamics to the same extent, and some cells even shift their Pd in the opposite direction, a fact that we cannot currently explain.

Shift of Pd and Adaptation

If the shift of Pd reflects adaptation to the new dynamics, it should also directly correlate with performance in the task. In particular, big shifts of Pd should correspond to well-adapted movements with small or no initial errors. To test this prediction, we analyzed cells one by one. We studied the correlation between the shift of Pd of SMA cells in the DT and the performance of the monkey in the task. Quantifying the goodness of adaptation (ADA) with the angle of initial deviation d, we divided all the trials in two groups: well-adapted trials (good ADA, $d \leq median(d)$) and poorly adapted trials (poor ADA, $d \geq median(d)$). We obtained two tuning curves for the two groups of trials, and we computed their Pd. We then evaluated the shift of Pd separately for the good ADA and poor ADA trials. As illustrated by the example in Figure 5, we found that good ADA trials had a greater shift of Pd than poor ADA trials. This adaptation effect was significant at the level of the population, as the good ADA Pd shifted significantly more than the poor ADA Pd (p < 0.03, circular bootstrap).

We performed this same analysis on the EMG activity of muscles recorded during the execution of movement. As expected, we found that greater shifts of Pd for muscles correlate with better adaptation (i.e., small d). Within our population of muscles, the good ADA Pd shifted significantly more than the poor ADA Pd (p < 0.005, circular bootstrap).

For neurons, we also analyzed the shift of Pd in relation to the stage of long-term learning (Figure 1E). We divided the 81 cells according to the mean initial deviation $\Delta \bar{d}$ (y axis in Figure 1E) into two subpopulations of neurons recorded in the early ($\Delta \bar{d} \geq median(\Delta \bar{d})$) and late sessions ($\Delta \bar{d} < median(\Delta \bar{d})$). We found comparable shifts of Pd for the early cells (n = 37; mean shift [±SD] = 9.9° [±6.1°]) and for the late cells (n = 44; mean shift [±SD] = 12.2° [±6.4°]). The recording sites for the two subpopulations essentially coincided.

Kinematics-to-Dynamics Transformation

Up to this point, we had analyzed the neuronal activity in the DT time window (i.e., the 0.5 s prior to the go signal). We had shown that in the DT, the individual and collective Pd of neurons in the SMA shifts in the direction of the external force when monkeys adapt to a perturbing force field. We then analyzed the time course of that shift of Pd within the delay. For this analysis, we aligned all the trials with the presentation of the cue signal and computed the Pd in sliding time bins of 300 ms width.

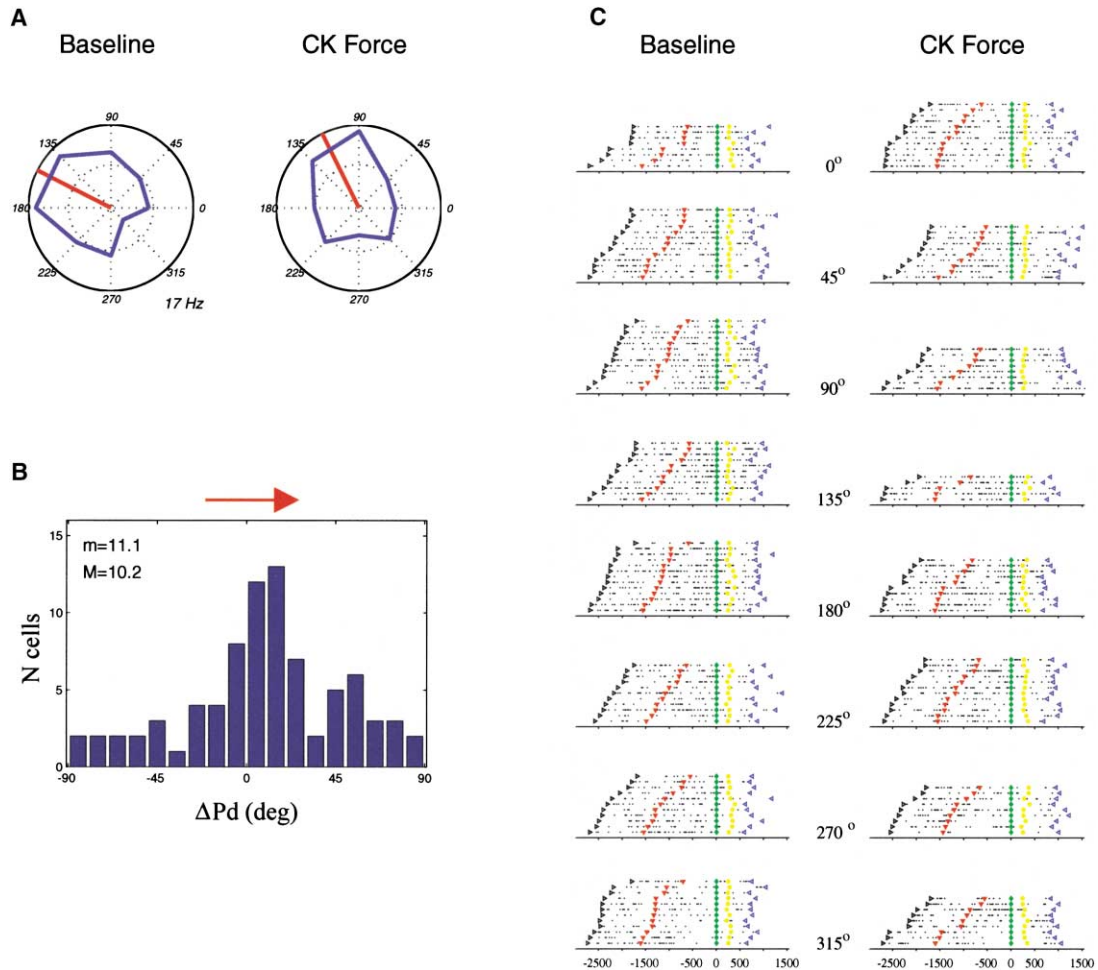Figure 6 illustrates the results obtained for the popula-

Figure 3. Shift of Pd in the Delay Time (DT)

(A) Tuning curve of one cell. The activity of the cell recorded in the 0.5 s prior to the go signal is plotted in blue in polar coordinates. The preferred direction (Pd) is indicated in red. The same scale of 17 Hz is used for the two plots. The internal circle (black broken line) indicates the average activity at rest (i.e., during 0.5 s preceding the cue signal).

(B) Population. The histogram represents the shift of Pd between the force condition and the baseline condition. The last 0.5 s before the go signal are considered here (DT time window). Positive values on the x axis indicate shifts in the direction of the external force. The "m" and "M" are the mean and median of the histogram, respectively. As a population, neurons show a significant shift (p < 0.02, t test).

(C) Raster plots of one cell (same cell as in [A]). Each dot is one spike, and the colors indicate the beginning of the trial (black), the presentation of the cue signal (red), the go signal (green), the movement onset (yellow), and the movement end (blue). The trials were aligned at the go signal and ordered according to the duration of the delay for the eight movement directions (rows) and for the two conditions (columns).

tion of 81 cells. The x axis represents the time (t), and the cue signal was presented at time t = 0. The y axis represents the shift of Pd, with positive values indicating shifts in direction of the external force. Each data point represents the mean shift of Pd (or collective shift of Pd) recorded for the population in the 300 ms bin centered in the corresponding time t (the vertical bars are standard deviations). Because we considered only the activity prior to the go signal, the rightmost data points are computed from fewer trials. Zero on the y axis is the Pd in the baseline condition for the last time bin considered (t = 850 ms, one-half of the trials).

In the baseline condition (Figure 6, left), the collective Pd of SMA cells remains essentially constant throughout the delay (with some variance at the beginning; see below). In the force condition (Figure 6, right), the collective Pd of SMA cells is initially aligned with that in baseline. Over the course of the delay, however, the collective Pd progressively shifts toward the direction of the external force. Since in the force condition the shift of Pd reflects the new dynamics and the absence of that shift reflects the desired kinematics, we interpret the progressive shift of the collective Pd in Figure 6 (right) as a neuronal correlate of the KD transformation.

According to our interpretation, neurons in the SMA process the KD transformation both in the baseline and force conditions. The KD transformations computed in the two conditions differ from each other only with respect to the dynamics. In the baseline, the desired kinematics and the dynamics are aligned, and the collective
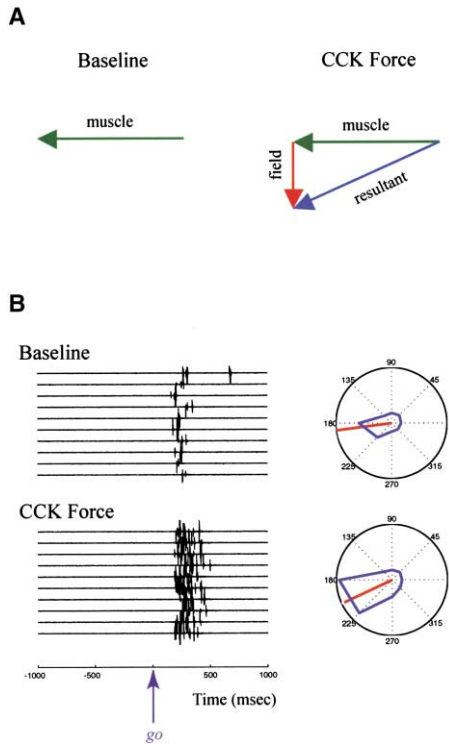
A

B

Figure 4. Muscles EMG Activity

(A) Changes of muscular Pd under adapted conditions (cartoon). In the baseline condition, the only force exerted upon the hand of the monkey is that of muscles. In particular, we can consider one muscle (muscle x) with Pd oriented toward 180°. In other words, when muscle x is active at its maximum in the baseline condition, the hand moves toward the left. How will the Pd of muscle x change in the force condition when the monkey adapts to a CCK force field? When muscle x is active at its maximum in the force condition, two forces are exerted upon the hand: the force of muscles (green) and the perturbing force (red). These two forces vector-sum, and the resultant force (blue) indicates the direction in which the hand moves. In other words, the new Pd of muscle x is now shifted CCK (i.e., in the direction of the external force) compared to the old Pd. And the same is true for any muscle, irrespectively of the initial Pd.
(B) Actual muscle (Biceps). Left: EMG traces. Movements toward 225° are aligned at the go signal. Notably, there is no EMG activity in the delay. Right: tuning curve plotted in polar coordinates. In the force condition, the Pd (red) shifts in the direction of the external force (CCK).

Pd remains essentially constant throughout the delay. In the force condition, the same desired kinematics is associated to a new dynamics, and as the KD transformation occurs, the collective Pd gradually shifts.

KD Transformation of Individual Neurons
Progressive shifts of Pd are also observed at the level of single neurons. The three panels in Figure 7 illustrate the activity of three different cells, in a format similar to that of Figure 6. For each cell in Figure 7, however, the Pd in the force condition (red color) is superimposed on the Pd in the baseline (black color). It is worth noting that the Pd of single neurons is not constant throughout the delay in either the baseline or the force condition (Johnson et al., 1999). This nonconstancy of Pd ob-

served for single cells, however, averages out when we consider the population in baseline (Figure 6A). The key point of Figure 7 is that for all three cells, the Pd in the force condition is initially close to that in the baseline and progressively departs from it over the course of the delay. This suggests that individual neurons in SMA might process the KD transformation.

Quantitatively, we investigated whether the cells that process the new dynamics in the force condition also reflect the KD transformation. In other words, we investigated whether the cells that shift their Pd in the force condition do so progressively over the course of the delay. To identify these cells, we imposed the arbitrary criterion that the shift of Pd in the DT time window be above average (11.1°); a total of 36 cells satisfied this criterion.

For each of these cells and for each 300 ms time bin centered on time t (time bins as in Figure 7), we computed the difference, $\Delta Pd(t)$, between the Pd in the force condition and the corresponding Pd in the baseline condition. We then stated whether the shift of Pd was progressive using a linear regression analysis (regression of $\Delta Pd(t)$ on t). We found that the slope of the regression line was significantly positive ($p < 0.01$) for 31% of the cells (10/32), indicating that the shift of Pd had occurred progressively during the delay. In contrast, the slope of the regression line was significantly negative for only 6% of the cells (2/32). This result is very unlikely ($p < 10^{-4}$, multinomial test) if positive and negative slopes occur with equal probability (i.e., if significantly positive slopes occur at random). Thus, this analysis supports the suggestion that the KD transformation can be traced to the activity of individual neurons.

Shift of Pd and Reaction Time
Finally, we studied the correlation between the shift of Pd measured in the DT time window and the reaction time (RT). The rationale for this analysis was that the KD transformation may or may not be fully processed before the go signal. If the KD transformation is concluded prior to the go signal, then the RT should only include the time necessary for the monkey to initiate the movement. If the KD transformation is not concluded prior to the go signal, then the motor system of the monkey should conclude it first, before initiating the movement. If the shift of Pd of the SMA neurons is indeed a measure of the state of the KD transformation, then we may expect big shifts of Pd to correlate with short RT and small shifts of Pd to correlate with long RT (see also Riehle and Requin, 1993).

Quantitatively, we investigated whether cells that shift their Pd during the DT time window do so more extensively prior to short RT than prior to long RT. Again, we restricted this analysis to the cells whose shift of Pd in the DT time window was above average (36 cells). For each of these cells, we divided the trials in the force condition into two groups according to the RT: short RT trials (RT $\leq$ median(RT)) and long RT trials (RT $\geq$ median(RT)). We then computed the shift of Pd separately for the two groups of trials. Figure 8A illustrates the results obtained for one particular cell. When all the trials are considered (all RT, data not shown), the Pd shifts by 19° in the force condition compared to baseline.

A

Baseline   CK Force

good ADA

poor ADA

22 Hz

B

C

Baseline   CK Force
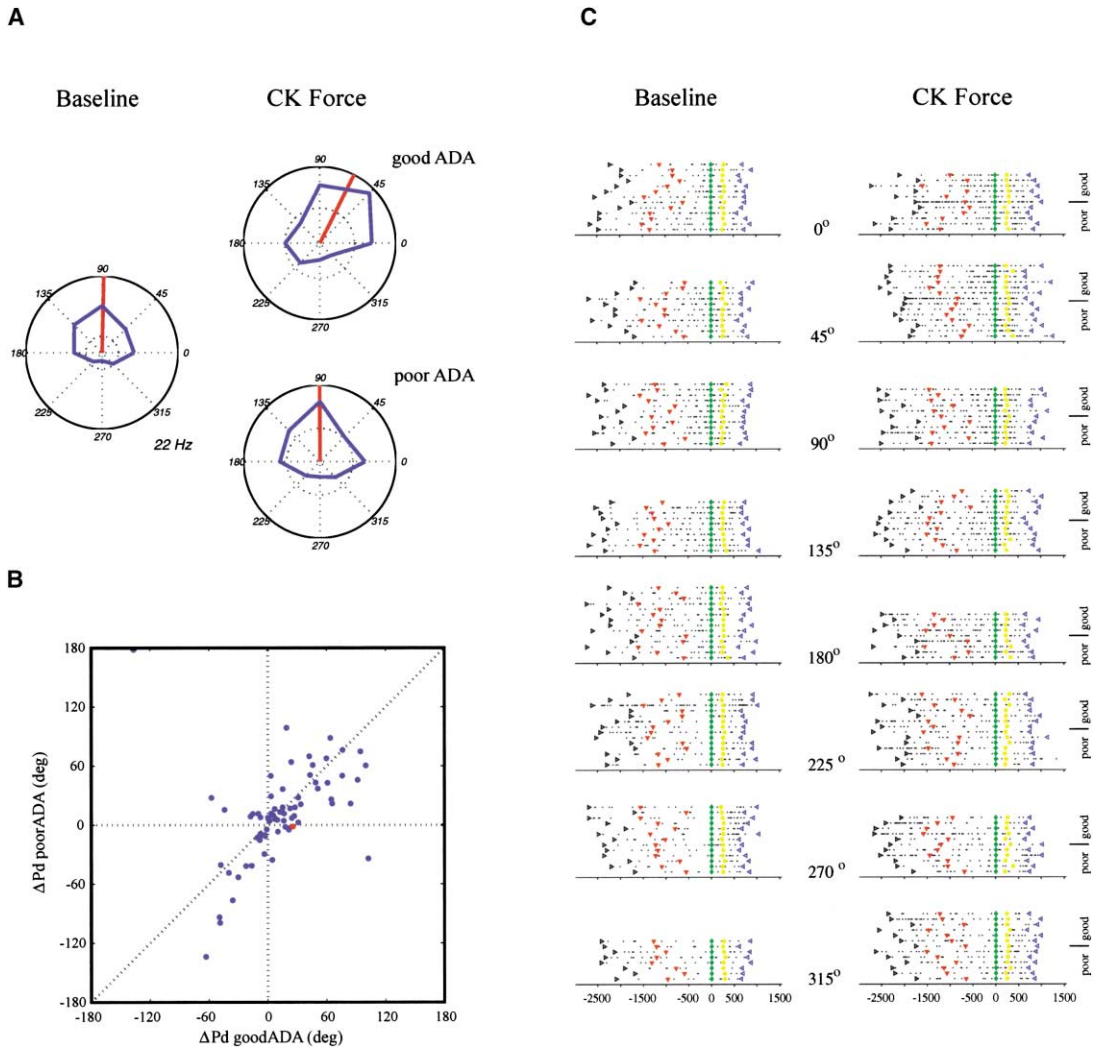
0°
45°
90°
135°
180°
225°
270°
315°

Figure 5. Adaptation Effect

(A) Adaptation effect, one cell. The plot on the left illustrates the activity recorded in the baseline condition (all trials are considered.) The plots on the right illustrate the activity recorded in the force condition prior to well-adapted trials ($d \leq$ median(d), top) and poorly adapted ($d \geq$ median(d), bottom). This cell was recorded with a CK force field. It can be seen that there is a more pronounced shift of Pd for good ADA trials than for poor ADA trials. In other words, when at the end of the delay the Pd has shifted more, the movement that follows is well adapted (good ADA). When the Pd has shifted less, the movement that follows is poorly adapted (poor ADA). The activity in the last 0.5 s prior to the go signal was considered here, and the same scale of 27 Hz was used for the three plots. All other conventions are as in Figure 3A.

(B) Adaptation effect, population. In this plot, each point represents one cell. The x axis represents the shift of Pd for the good ADA trials and the y axis represents the shift of Pd for the poor ADA trials. Although some variability is present, it can be noted that the population tends to lie below the diagonal line (p < 0.03). The cell shown in (A) is indicated in red.

(C) Raster plots of the cell shown in (A). Color codes are the same as in Figure 3A. In this case, trials were aligned at the go signal and ordered according to the initial deviation d.

When the short RT and long RT trials are computed separately, the shift is more pronounced for the short RT (24°) than for the long RT (10°). We refer to this phenomenon as the RT effect. As shown in Figure 8B, the RT effect was consistent across cells (p < 0.03, circular bootstrap).

The SMA and Other Areas
The kinematics-to-dynamics transformation is a crucial operation necessary for executing visually instructed reaching movements. It would therefore seem somewhat odd if this process were entirely accomplished within one area in which a lesion does not prevent simple movements (Chen et al., 1995; Thaler et al., 1995; Tanji et al., 1985). Thus, our results by no means suggest that the neuronal processing of the KD transformation is confined to the SMA. However, our data do imply that movement dynamics can be partly processed during motor planning, well before the initiation of the movement. They also testify that some neurons in the SMA
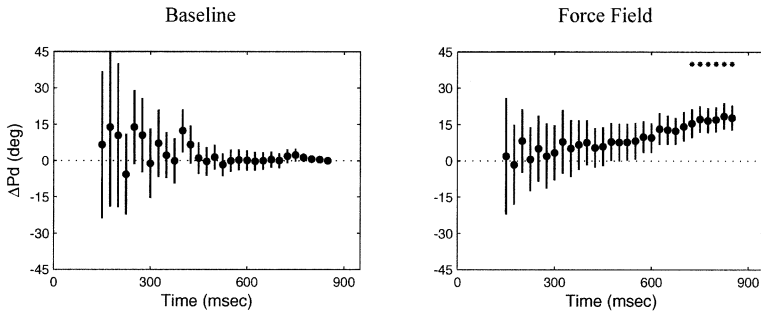
Baseline

Force Field

Figure 6. Time Course of the Pd Shift: Population

Time evolution of the Pd: population. We aligned trials with the cue signal (time = 0) and computed the Pd in 300 ms time bins (every 25 ms). Positive values on the y axis indicate shifts of Pd in the direction of the external force. Solid points and vertical bars indicate the mean and standard deviations. Asterisks indicate data points significantly greater than zero ($p < 0.01$, t test). In the baseline condition, the collective Pd remains essentially constant throughout the delay. In the force condition, the collective Pd is initially aligned with that recorded in baseline and progressively shifts over the course of the delay in the direction of the external force. A linear regression analysis (of $\Delta Pd(t)$ on t) indicated that the 26°/s slope found in the force condition (linear fit) was significantly greater than zero ($p < 10^{-9}$). Only the activity preceding the go signal was considered here. (Thus, data points with $t > 500$ ms are based on fewer trials.) The large error bars early in the delay are due to the nonconstancy of Pd seen for single cells (Figure 7).

may participate in the processing of the KD transformation.

To investigate the contribution of other cortical motor areas, we undertook recordings from the primary motor cortex (M1; Li et al., 2001), and the dorsal premotor area (PMd or F2) and the ventral premotor area (PMv) (J.X., C.P.-S., and E.B., unpublished data). Recent anatomical work has shown that all these areas have direct projections to the spinal cord (He et al., 1993; 1995), leading to the hypothesis that movements may not be controlled in a strictly serial fashion. Consistent with this hypothesis, a preliminary analysis of our data suggests that the phenomena described here are not unique to the SMA. A total of 162 M1 cells, 142 PMd cells, and 143 PMv cells were available for analysis. With respect to the 0.5 s prior to the go signal (DT time window), we observed a pronounced activation in the PMd (41/142 cells) where the shift of Pd reaches significance (mean shift 10.4°, $p < 0.05$, circular t test). In contrast, we found little delay activity and no significant shift in M1 (16/162 cells; mean shift 4.9°, $p = 0.4$, circular t test) and in PMv (17/143 cells; mean shift 3.1°, $p = 0.8$, circular t test). With respect to the activity during the execution of movement, however, we found significant shifts of Pd in all four areas: PMd (43/142 cells; mean shift 11.8°, $p < 0.02$, circular t test,

SMA (128/252 cells; mean shift 16.0°, $p < 10^{-5}$, circular t test), M1 (62/162 cells; mean shift 16.2°, $p < 10^{-5}$, circular t test), and PMv (41/143 cells; mean shift 15.1°, $p < 0.03$, circular t test). Thus, the neuronal processing of the KD transformation may involve several motor areas.

Discussion

In this study, we have recorded and analyzed the activity of neurons in the SMA prior to and during visually instructed reaching movements. We have contrasted the activity in nonperturbed conditions (baseline) with that recorded in the presence of a perturbing force to which the monkeys adapted (force condition). As in many previous studies, we have interpreted force-dependent neuronal activity as reflecting movement dynamics and force-independent neuronal activity as reflecting movement kinematics (Evarts, 1968; Thach, 1978; Kalaska et al., 1989, 1990; Crutcher and Alexander, 1990; Alexander and Crutcher, 1990a, 1990b; Li et al., 2001). Specifically, the curl force fields used here reduce that force dependence to changes in one parameter, the preferred direction (Pd). In the presence of curl force fields, the Pd shifts in the direction of the external force. The novelty
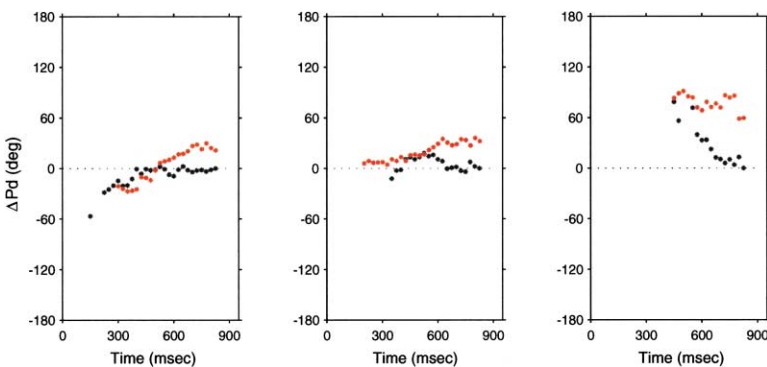

Figure 7. Time Course of the Pd Shift: Single Cells

KD transformation for single cells. The three panels illustrate the activity of three different cells. We aligned trials at the cue signal (time = 0, x axis), and we computed the Pd (y axis) in 300 ms time bins shifted by 25 ms from each other only for directionally tuned activity. In the plots, for each cell we superimposed the Pd in the baseline (black) onto that in the force condition (red). "Zero" on the y axis is the Pd in the baseline condition recorded in the rightmost time bin (t = 850 ms), and positive values on the y axis indicate shifts of Pd in the direction of the external force. In all three cases, it can be noticed that the Pd in baseline does not remain constant throughout the delay. However, the variability of Pd recorded for different cells averages to zero when we consider the entire population (Figure 5A). Consider now the cell on the left panel. In the force condition, the initial value recorded for the Pd after the cell becomes tuned is close to the corresponding value in the baseline. Over the course of the delay, however, the Pd in the force condition progressively departs from that in baseline. The other two cells in the center and right panels show similar trends: their Pd in the force condition are initially aligned with the Pd in baseline and progressively depart from them over the course of the delay. This indicates that the physiological correlates of the KD transformation can be traced to the activity of single neurons. Note that since we only considered the activity prior to the go signal, the rightmost data points in each plot are computed from fewer trials.
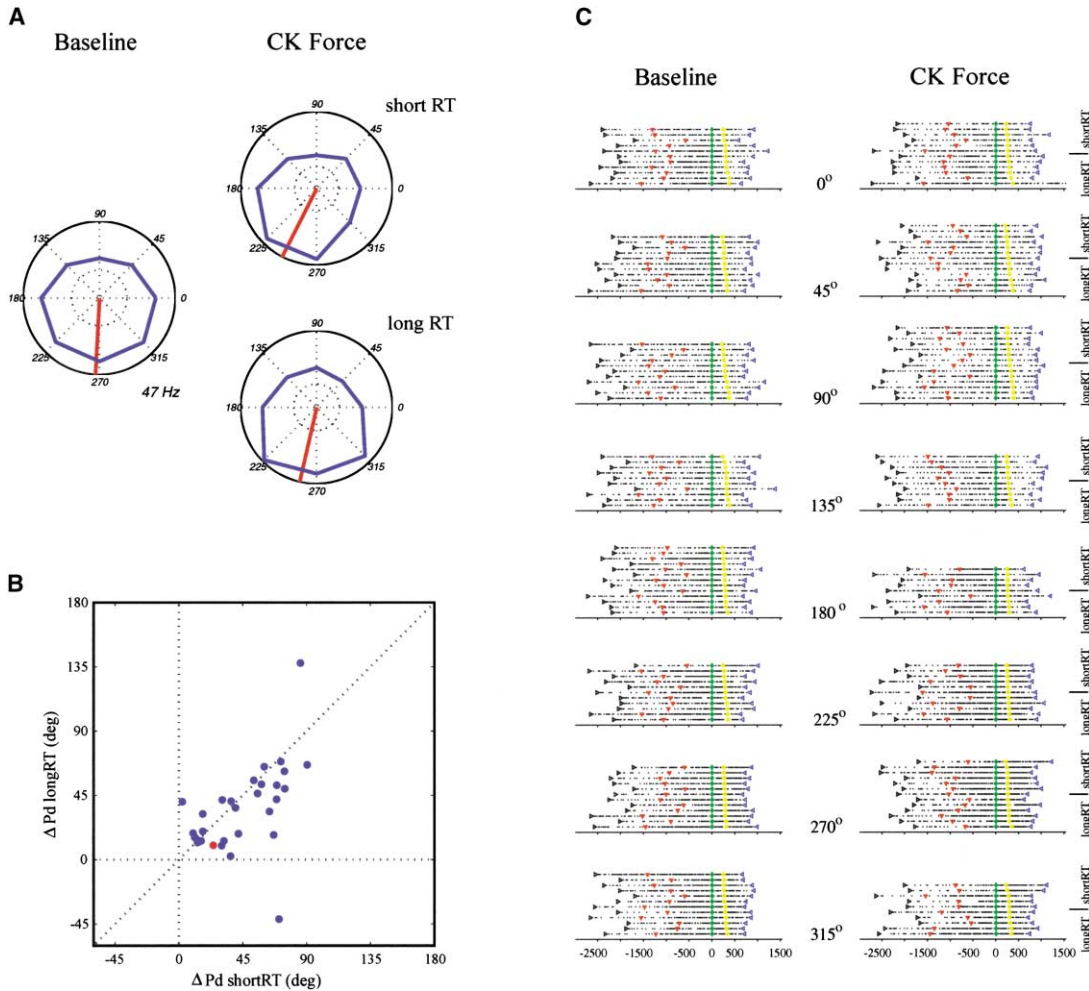
Figure 8. Reaction Time Effect

(A) RT effect, one cell. The left plot illustrates the activity recorded in the baseline condition. (All trials are considered.) The right plots illustrate the activity recorded in the force condition, separately for trials with short RT (RT ≤ median(RT), top), and long RT (RT ≥ median(RT), bottom). The cell was recorded with a CK force field. It can be seen that the shift of Pd is more pronounced for short RT trials than for long RT trials (RT effect). Thus, when the state of the KD transformation at the end of the delay is more advanced (larger Pd shift), a shorter RT is sufficient to initiate the movement after the go signal. When the state of the KD at the end of the delay is less advanced (smaller Pd shift), a longer RT is necessary to initiate the movement after the go signal. The activity in the last 0.5 s prior to the go signal was considered here, and the same scale of 47 Hz was used for the three plots. All other conventions are as in Figure 3A.

(B) RT effect, population. In this plot, each point represents one cell, and the cell shown in (A) is indicated in red. The x axis represents the shift of Pd for the short RT trials. The y axis represents the shift of Pd for the long RT trials. It can be seen that the population tends to lie below the diagonal line (p < 0.03), indicating that the RT is consistent for the population of cells that process the dynamics of the upcoming movement during motor planning.

(C) Raster plots of the cell shown in (A). Color codes are the same as in Figure 3A. In this case, trials were aligned at the go signal and ordered according to the RT.

of the present study is that we have investigated the activity during a delay interposed between the instruction (cue signal) and the go signal.

We have presented two main results. First, the dynamics of the upcoming movement was reflected in the activity of some neurons in the SMA before the go signal. Second, over the course of the delay, neurons in the SMA progressively came to reflect the dynamics rather than the desired kinematics of the upcoming movement. This result, obtained both for individual neurons and for the population, suggests that neurons in the SMA participate in the kinematics-to-dynamics (KD) transformation. Two independent measures of correlation sup-

port this suggestion. First, the dynamics computed during the instructed delay, as reflected in the activity of SMA neurons, correlates with the initial direction of the upcoming movement (adaptation effect). Second, the state of the KD transformation at the end of the delay, as reflected in the activity of SMA neurons, anticorrelates with the following reaction time (RT effect).

Present and Previous Observations
It can be noted that the RT effect implies in principle the progressive shift of Pd. If big/small shifts of Pd are found before short RT/long RT (RT effect), then the shift of Pd was not constant but presumably was increasing

over the course of the delay (KD transformation). It is therefore particularly interesting to note the RT effect in previously published data. In their study, Alexander and Crutcher (1990a) trained monkeys in an assistive/null/resistive load task and found a significant effect of loads during the delay for 20% of SMA cells. Although their conclusions partly differ from ours, the cell shown in their paper (right side of Figure 9 in Alexander and Crutcher, 1990a) has the characteristics described in the present article. The activity of the cell is directional (it is higher before extension than before flexion) and load dependent (it is higher before opposed movements than before assisted ones). Moreover, inspection of the activity preceding opposed movements reveals a clear RT effect. Specifically, the RT effect can be seen by comparing the delay activity in the top five trials (short RT, higher activity) with that in the bottom five trials (long RT, lower activity). The RT effect is also evident in the load-dependent SMA cell shown by Alexander and Crutcher in the second paper of their series (Figure 3 in Crutcher and Alexander, 1990).

Neuronal Processing of Movement Dynamics
According to the traditional view, the premotor areas of the frontal lobe harbor high sensorimotor processes and feed the primary motor cortex (M1), which executes the movement through its anatomical projections to the spinal cord. This serial view was recently challenged on the basis of anatomical studies, showing that direct projections to the spinal cord originate from multiple areas including the SMA, the cingulate motor areas, PMd, PMv, and M1. Moreover, physiological studies designed to dissociate between different aspects of the movement have generally found extensive functional overlaps. These observations lead to the proposal that different motor areas may contribute to the control of movement largely in parallel. Our data speak to this issue in two respects. First, we confirmed that neurons in the SMA (and PMd and PMv) reflect the movement dynamics, a late computational stage, as neurons in M1 do. Second, we found evidence of dynamics-related activity in the SMA (and PMd) during the phase of motor planning as well. In contrast, no such evidence was found in M1 (and PMv). Taken together, these results suggest that although a strictly serial view is probably inadequate, different areas of the frontal lobe contribute differentially to the control of movement.

Several authors have proposed that the cerebellum plays an important role in the acquisition and storage of new internal models of the dynamics. The present data are not inconsistent with such a proposal and leave open at least two possible scenarios. One possibility is that the internal model for the dynamics is indeed stored only in the cerebellum and that the motor areas of the frontal lobe, including the SMA, load the dynamics when necessary. In this case, the KD transformation observed here represents that gradual loading of the dynamics by neurons whose activity is initially purely kinematics related. Another possibility is that the internal model for the dynamics is stored in the synapses of multiple areas including the SMA and that the progressive KD transformation here observed represents an actual computation. In this view, the KD transformation is processed

with the contribution of multiple areas including the SMA and other premotor areas of the frontal lobe, the cerebellum, and possibly the basal ganglia. Hopefully, future work will contrast these hypotheses.

Our data also help to clarify one of the roles of the SMA in the control of movement. A motor area in the frontal medial wall was discovered and named the "SMA" 50 years ago (Penfield and Welch, 1951; Woolsey et al., 1952). More recently, however, that "SMA" was divided into a rostral preSMA (or F6) and a caudal SMA-proper (or SMA or F3) (Matelli et al., 1991; Luppino et al., 1991; Matsuzaka et al., 1992; Shima and Tanji, 2000). The present study was carried out on the SMA-proper (or just SMA). Among other differences, the preSMA and the SMA are distinguished by their anatomical projections because the SMA projects directly to the spinal cord and to M1 (He et al., 1995; Wise, 1996), whereas the preSMA lacks such projections. The undivided "SMA" was originally thought to harbor early sensorimotor processes and complex motor functions. However, subsequent studies have assigned these high functions to the preSMA (Matsuzaka et al., 1992; Hikosaka et al., 2000; Picard and Strick, 1996; Shima and Tanji, 2000). Our data implicate the SMA in a rather late computation, the movement dynamics. If extended to the other premotor areas of the frontal lobe with direct projections to the spinal cord, namely PMd, PMv, and the cingulate motor areas, this finding would provide a physiological counterpart for the most recent anatomical maps (He et al., 1993, 1995).

Finally, the presence of dynamics-related activity in PMd and SMA during motor planning is consistent with the remarkable observation of delay-time activity in spinal interneurons (Prut and Fetz, 1999). It also suggests an alternative interpretation for the mental rotation of the neuronal population vector observed in M1 before initiation of kinematics-adapted movements (Georgopoulos et al., 1989).

Multistage Processing of the Movement Dynamics
Although our results, in particular the adaptation effect and the RT effect, suggest a close association between the activity of neurons in the SMA and the motor output performance, the level of causality between that neuronal signal and the movement remains undetermined. The viscous perturbation used in the experiment was null in the delay, weakest at the onset of the movement, and gradually increased in the early phase of the movement. Considering that movements were not overcompensated on average (as quantified by the initial deviation d, see Table 1), it may appear counterintuitive that neurons in the SMA show a substantial shift of Pd prior to the go signal. One possibility is that the dynamics-related activity in the SMA refers to a larger portion of the movement, not just the beginning of it. Thus, the signal described here may refer to a weighted integral of the muscle forces f(t) over time, for example, with exponentially decaying weights. This view corresponds to the psychophysical intuition that movements are not planned in small portions. Another possibility is that the shift of Pd reflects the new dynamics (i.e., the forces exerted by the muscles) only in an abstract sense, as

Table 1. Average Reaction Time and Perpendicular Displacement

	Baseline	Force
Mean RT: all RT (ms)	284 ($\pm$16)	283 ($\pm$16)
Short RT	258 ($\pm$14)	257 ($\pm$15)
Long RT	308 ($\pm$19)	309 ($\pm$19)
Mean d: all ADA (mm)	-0.2 ($\pm$0.8)	0.4 ($\pm$1.1)
Good ADA	-1.0 ($\pm$0.8)	-0.5 ($\pm$1.2)
Poor ADA	0.7 ($\pm$0.8)	1.4 ($\pm$1.1)
Correlation (RT, d)	-0.04 ($\pm$0.12)	-0.01 ($\pm$0.12)
Movement duration (ms)	606 ($\pm$121)	677 ($\pm$91)

For each session, we computed the mean RT and mean d for the different groups of trials. The data reported are averages across sessions ($\pm$SD). For the initial deviation d, positive values correspond to deviations in the same direction as the force field. The correlation is computed session by session and averaged across sessions. The movement duration is the time from the onset of movement to its end. Note that the correlation between RT and d is negligible in both conditions.

a symbolic representation of the different associations between sensory stimuli and motor output in the two conditions or as a dynamic goal. In either case, the question remains as to how hierarchically lower circuitry decode and filter the signal observed here and then transform it into the proper input to the motoneurons. In this respect, our data are consistent with the hypothesis that the movement dynamics is processed in multiple stages. In this view, the dynamics-related signal recorded here in the SMA represents the most remote of these processing stages.

The hypothesis that movement dynamics is a process involving multiple neural steps is at variance with the equilibrium-point model. According to the most simple formulation of the equilibrium-point hypothesis, the CNS specifies a posture through the choice of muscle length-tension curves that set agonist-antagonist torque-angle curves determining an equilibrium position for the limb and a stiffness about the joints. Arm trajectories are generated through a control signal defining a series of equilibrium points (Bizzi et al., 1984). Because the neuromuscular system is spring-like, the instantaneous difference between the arm's actual position and the equilibrium position specified by the CNS can generate the requisite torques, avoiding the complex inverse dynamics problems of computing the torques at the joints (Bizzi et al., 1992). In contrast, the present results are consistent with new discoveries on the modular organization of the spinal cord (Giszter et al., 1993; Bizzi et al., 2001). In the emerging model, supra-spinal signals conveying information about the impending dynamics activate the modular interneuronal circuitry of the spinal cord, thus generating force fields that have been shown to combine vectorially (Mussa-Ivaldi et al., 1994).

Interpretative Concerns

We considered two alternative interpretations of our results. One possibility is that monkeys deal with the perturbing force by adopting a different strategy than that hypothesized here. In particular, monkeys could aim at a virtual target slightly shifted in the direction opposite to the force field compared to the actual target (the movement endpoint). In this case, the adaptation would

consist of remapping the visual stimulus onto a new desired target, similar to what presumably occurs when experimenters deliberately manipulate that mapping (Wise et al., 1992; Shen and Alexander, 1997). We further investigated this virtual-target hypothesis with a model by simulating the trajectories the hypothesis predicts and by comparing them with the trajectories actually recorded during the experiments. Assuming that in the force condition monkeys plan straight-line trajectories akin to those observed in the baseline condition, the virtual-target hypothesis predicts overcompensated movements. In other words, if the monkeys actually aimed at a visual target slightly displaced in the direction opposite to the external force, their hand trajectory would start off directed toward that virtual target and, under the effect of the force field, would gradually land over the actual target. In contrast, the hand trajectories actually recorded during the experiments are slightly undercompensated, as quantified by the initial deviation d (see Table 1, Figure 1E). This argues against the virtual target hypothesis.

Another possibility is that the progressive shifts of Pd shown in Figures 6 and 7 mark the transformation from the old dynamics to the new dynamics (KDD' hypothesis). In this view, adapted movements would require one extra mental operation (Cisek and Scott, 1999). In the baseline condition, monkeys would simply transform the desired kinematics into the old dynamics (KD). In the force condition, they would first transform the desired kinematics into the old dynamics (KD) and then transform the old dynamics into the new dynamics (DD'). Although we cannot definitively exclude the KDD' hypothesis, we view it as unlikely, based on the following two considerations. First, the analysis of the reaction time (RT) suggests that neither the computation of D' in the force condition nor the computation of D in baseline are completed before the go signal. (On the one hand, there would be no RT effect if D' was fully computed before the go signal in the force condition. On the other hand, the average RT is almost identical in the two conditions, suggesting that whatever is left to compute after the go signal in the force condition is also left to compute after the go signal in the baseline.) Second, Figure 6 suggests that if a KD transformation is ever processed in the force condition, that transformation is concluded early in the delay (say within 350 ms after the cue signal). Thus, the KDD' hypothesis implies that the same KD transformation takes place in very different time courses in the two conditions: throughout the delay and beyond the go signal in the baseline, early after the cue signal in the force condition. Moreover, the difference between the time of the KD transformation in the two conditions would exactly equal the time necessary for the DD' transformation in the force condition, a somewhat odd coincidence. We therefore prefer the established understanding (Alexander and Crutcher, 1990a; Shadmehr and Mussa-Ivaldi, 1994; Kawato, 1999; Bhushan and Shadmehr, 1999) that, when performing adapted movements, monkeys transform the desired kinematics directly into the new dynamics (KD' hypothesis). According to this view, the transformations taking place in the baseline and force conditions are equivalent except for D being substituted by D' in the force condition, a simple account for our data. This interpretation is also supported by data showing similar

PET (Positron Emission Tomography) activation in the human SMA before and after adaptation to the force field (Shadmehr and Holcomb, 1997).

Finally, we think that the progressive shifts of Pd in Figures 6 and 7 do not just represent a preview of the time-varying force perturbation because the duration of the delay was randomly variable (0.5–1.5 s), and trials in Figures 6 and 7 were aligned at the presentation of the cue signal (i.e., not with any aspect of the movement such as the movement onset).

Force Independence and Desired Kinematics

In Figures 6 and 7, we have interpreted a signal evolving from force independence to force dependence as a correlate of a kinematics-to-dynamics transformation. Yet, the desired kinematics was not the only quantity that remained unchanged across conditions. Specifically, any computation (such as processing of the visual stimulus, the decision, the target or goal, or the inverse kinematics) prior to the movement dynamics was not influenced by the force. In addition, variables related to eye position (which we did not measure) were likely to be independent of the force. The reason for our interpretation is that the desired kinematics is presumably the last computational stage prior to the dynamics. Excluding that a processing stage preceding the desired kinematics (or related to eye position) is transformed directly into the movement dynamics, it can be assumed that the force-independent signals of Figures 6 and 7 also reflect the desired kinematics. In other words, although other force-independent variables may modulate it, it is unlikely that the activity of Figures 6 and 7 does not reflect the desired kinematics at all. In this respect, the progressive shift from force independence to force dependence is essentially related to a kinematics-to-dynamics transformation.

In contrast, it is unlikely that the force-independent activity shown in Figures 6 and 7 reflects the dynamics of putative muscles (for instance of the torso or the fingers) scarcely influenced by the perturbation. In principle, this is because the argument outlined in Figure 4A applies to any muscle having a significant directional tuning independent of what its contribution to the movement is. Moreover, that theoretical argument is supported by empirical evidence. In their experiments, Alexander and Crutcher recorded from a large number of muscles of the head, torso, hindlimb, forelimb, and hand, and found that the EMG activity of 38 out of 39 muscles was changed by the external load (Crutcher and Alexander 1990). In other words, the activity of muscles is never force independent.

Neuronal Correlates of a Transformation

Although numerous studies have suggested the occurrence of sensorimotor transformations (among others, Alexander and Crutcher, 1990a, Andersen et al., 1993; Shen and Alexander, 1997; Olson and Gettner, 1995; Duhamel et al., 1997; Colby, 1998; Graziano et al., 1994; Hernandez et al., 2002), the evidence for their neuronal correlates was generally indirect. One interesting aspect of our results is that the correlates of a transformation, i.e., the KD transformation, are described in real time. One important aspect of our paradigm is that because

shifts of Pd in the same direction are imposed onto many neurons, we can analyze the changes simultaneously for the entire population (i.e., with a higher statistical power). Nonetheless, we find it particularly intriguing that correlates of the KD transformation are found–at least in some cases–also at the level of individual neurons. Indeed, sensorimotor transformations (as well as other transformations) could in principle be processed in the CNS by neuronal subpopulations activating one after the other. Instead, we found individual neurons that reflected the dynamics in a progressively increasing fashion, starting from a kinematics-related signal. One interesting question that remains is whether other transformations can also be traced to the activity of individual neurons.

Experimental Procedures

Behavioral Task

Two male rhesus monkeys (*Macaca mulatta*), C and F, participated in the experiment, and both performed with the right arm. The experimental setup and behavioral paradigm were essentially the same as described in Li et al., 2001. The monkey sat on a chair in an electrically insulated enclosure and held the handle of a robotic arm with two degrees of freedom. A computer monitor placed 75 cm in front of the monkeys indicated with a cursor (3 × 3 mm square, 0.2° visual angle) the position of the handle and the targets of the externally instructed movements (16 × 16 mm squares, 1.1° of visual angle). The monkey's movements were confined to a horizontal plane. In each trial, a center square appeared on the monitor, and the monkey moved the cursor into the center square to initiate the trial. After 1 s, a peripheral target (cue signal) appeared randomly at one of eight locations around the clock. The monkey held the cursor within the center square for a randomly variable period of time (delay) of 0.5 to 1.5 s. The center square was then extinguished (go signal). The monkey had to move and acquire the peripheral target within 3 s and to remain within the peripheral target for 1 s to receive a juice reward. Movements were 8 cm in length, and the monkey was required to make movements within the spatial window confined to 60° on both sides of the line passing through the center square and peripheral target.

Two motors at the base of the robot could exert perturbing force fields upon the hand of the monkey. We used curl viscous force fields $F = BV$ with $B = [0-b; b\ 0]$ and $b = \pm0.06$ N sec/cm. Depending on the sign of b, the field was clockwise (CK) or counterclockwise (CCK). Monkeys were trained in the nonperturbed reaching task (4–6 months), and the force fields were only introduced during the recordings. In each session, the monkey performed in the baseline and force conditions, followed by a washout condition where the forces were removed. Each condition included approximately 20 successful trials per movement direction. For monkey C, sessions with the two force fields were run in blocks (27 and 28 sessions, respectively), starting with the CK force field. Monkey F was tested on the CCK force field only (40 sessions). The present analysis focused exclusively on the baseline and force conditions.

Recordings

The SMA was identified and distinguished from the preSMA through electrical microstimulation (monkey C) and histology (monkey F). For microstimulation, we used a train of 20 biphasic pulse pairs (width = 0.1 ms, duration = 60 ms) at 330 Hz and 10–40 μA. For the histology, we marked the recording sites with electrolytic lesions (cathodal current, 20μ A, 2 min). After euthanasia, the brain was photographed, sectioned (coronal plane, 28 μm sections), and Nissl-stained. Recordings electrodes were placed in the medial wall, caudal to the alignment with the genu of the arcuate sulcus. Microscopic inspection revealed that the recording region was poorly laminated and lay within 6 mm rostral to tissue displaying a single line of giant pyramidal cells (Matelli et al., 1991). Hand trajectories were recorded at 100 Hz and saved for analysis. Neuronal recordings followed standard procedures. Up to eight vinyl-coated tungsten electrodes

(1–3 MΩ impedance) were independently advanced by manually rotating a threaded rod screw (300 μm/turn). The neuronal activity was recorded (Experimenter's Workbench 5.3, DataWave Technology) and saved for analysis. For the electromyographic activity (EMG), we manually implanted bipolar wires during separate sessions. We recorded the EMG of the muscles pectoralis, deltoid, biceps, triceps, and brachioradialis (15 instances total). The EMG traces were rectified, integrated over the movement-related time window, averaged across trials, and submitted to the same analysis as cells.

The NIH guidelines on the use of animals were followed throughout the experiment.

Data Analysis

From each trajectory $\mathbf{x}(t)=(x(t),y(t))$, we computed the speed $s(t)=||\dot{\mathbf{x}}(t)||$. The movement onset (mo) and movement end (me) were defined with threshold-crossing criteria on the speed (4 cm/s). We then defined the initial position (IP), the movement position (MP), and the final position (FP). IP was the average hand position in the 50 ms preceding the mo. MP was the weighted average of the hand position during the 500 ms following the mo, with exponentially decaying weights and time constant $\tau = 50$ ms. In formulas:

$$MP = \int_{mo}^{mo+500} \mathbf{x}(t)e^{-t/\tau}\, dt \Big/ \int_{mo}^{mo+500} e^{-t/\tau}\, dt$$

FP was the average hand position from the movement end to the delivery of the reward. The initial deviation d was defined as the angle between the line passing through IP and MP and the line passing through IP and FP. We defined d so as to obtain positive values $d > 0$ for movements deviated in the direction of the external force. For each session, we then computed the mean initial deviation $\Delta\bar{d} = \text{mean}(d)_{\text{force}} - \text{mean}(d)_{\text{baseline}}$.

To disregard the initial adaptation phase in the force condition, we excluded for each condition the first four successful trials in each movement direction. Only the remaining trials were considered for further analysis. Loose time constraints were imposed on the RT during the experiments. In the analysis, we excluded anticipatory movements (RT < 200 ms) and outliers (RT > 400 ms). The remaining trials were subjected to further analysis.

Neurons were identified through manual clustering (Autocut3, DataWave Technology). Their spiking activity was analyzed during the delay time (DT time window, defined as the 0.5 s prior to the go signal), and during the execution of movement (movement-related time window, defined from 0.2 s before the mo to the me). The same movement-related time window was used to analyze muscles.

The Pd was computed subject to the precondition of directional tuning (i.e., unimodal distribution of activity across directions) as revealed by the Rayleigh test (p < 0.01). The Pd was defined as the direction of the vector average of the eight directional activation. For the population analyses, we flipped the data recorded with the CK force field to obtain positive values when the Pd shifted in the direction of the external force. The statistical analysis followed standard methods. In particular, the collective Pd-shift for the population was stated with a nonparametric test for unimodal data (Fisher, 1993), which estimated the mean direction of small (circular bootstrap, p75) or large (circular t test, p76) samples. For the linear regression, we used a least-square-based method (Neter et al., 1985; p65).

We analyzed the adaptation effect of all the cells in the pool (81 cells), imposing the criterion that both the good ADA and the poor ADA tuning curves should pass the directional-tuning test (Rayleigh test). This criterion was satisfied by 75 cells.

The slope of the regression (Figures 6 and 7) was computed in the 300–800 ms following the cue signal. With respect to single neurons, the regression analysis was restricted to the cells whose Pd shift as measured at the end of the delay was above average (36 cells total). Only data points for which the Pd could be defined (i.e., the tuning curve was directionally tuned) were included in this analysis. To compute the slope, we also imposed the criterion that at least three data points be present (32 cells satisfied this criterion).

The analysis of the RT effect was restricted to cells with a Pd shift above average (36 cells). We also required that both the short

RT and long RT tuning curves passed the directional-tuning test (Rayleigh test; 30 cells satisfied this criterion).

For a control, we computed the population shift of Pd (Figure 3B) using a different criterion instead of the Rayleigh test as a precondition to compute the Pd. We tested the SMA population with the following preconditions, as previously used in other studies: ANOVA (p < 0.05 and p < 0.01), cosine tuning ($R^2 > 0.7$), adjustable width cosine ($R^2 > 0.7$, see Battaglia-Mayer et al., 2000), bootstrap (p < 0.01, see Crammond and Kalaska, 1996). All these tests, except that based on the strict cosine tuning, indicated a significant shift of Pd for the population.

References

Alexander, G.E., and Crutcher, M.D. (1990a). Preparation for movement: neural representations of intended direction in three motor areas of the monkey. J. Neurophysiol. *64*, 133–150.

Alexander, G.E., and Crutcher, M.D. (1990b). Neural representation of the target (goal) of visually guided arm movements in three motor areas of the monkey. J. Neurophysiol. *64*, 164–178.

Andersen, R.A., Snyder, L.H., Li, C.-S., and Stricanne, B. (1993). Coordinate transformations in the representation of spatial information. Curr. Opin. Neurobiol. *3*, 171–176.

Battaglia-Mayer, A., Ferraina, S., Mitsuda, T., Marconi, B., Genovesio, A., Onorati, P., Lacquaniti, F., and Caminiti, R. (2000). Early coding of reaching in the parietoccipital cortex. J. Neurophysiol. *83*, 2374–2391.

Bhushan, N., and Shadmehr, R. (1999). Computational nature of human adaptive control during learning of reaching movements in force fields. Biol. Cybern. *81*, 39–60.

Bizzi, E., Accornero, N., Chapple, W., and Hogan, N. (1984). Posture control and trajectory formation during arm movement. J. Neurosci. *4*, 2738–2744.

Bizzi, E., Hogan, N., Mussa-Ivaldi, F.A., and Giszter, S. (1992). Does the nervous system use equilibrium-point control to guide single and multiple joint movements? Behav. Brain Sci. *15*, 603–613.

Bizzi, E., Tresch, M.C., Saltiel, P., and d'Avella, A. (2001). New perspectives on spinal motor systems. Nat. Rev. Neurosci. *1*, 101–108.

Chen, Y.C., Thaler, D., Nixon, P.D., Stern, C.E., and Passingham, R.E. (1995). The functions of the medial premotor cortex. II. The timing and selection of learned movements. Exp. Brain Res. *102*, 461–473.

Cisek, P., and Scott, S.H. (1999). An alternative interpretation of population vector rotation in macaque motor cortex. Neurosci. Lett. *272*, 1–4.

Colby, C.L. (1998). Action-oriented spatial reference frames in cortex. Neuron *20*, 15–24.

Crammond, D.J., and Kalaska, J.F. (1996). Differential relation of discharge in primary motor cortex and premotor cortex to movements versus actively maintained postures during a reaching task. Exp. Brain Res. *108*, 45–61.

Crutcher, M.D., and Alexander, G.E. (1990). Movement-related neuronal activity selectively coding either direction or muscle pattern in three motor areas of the monkey. J. Neurophysiol. *64*, 151–163.

Duhamel, J.R., Bremmer, F., BenHamed, S., and Graf, W. (1997). Spatial invariance of visual receptive fields in parietal cortex neurons. Nature *23*, 845–848.

Evarts, E.V. (1968). Relation of pyramidal tract activity to force exerted during voluntary movement. J. Neurophysiol. *31*, 14–27.

Fisher, N.I. (1993). Statistical Analysis of Circular Data (Cambridge, MA: Cambridge University Press).

Flanagan J.R., Nakano, E., Imamizu, H., Osu, R., Yoshioka, T., and Kawato, M. (1999). Composition and decomposition of internal models in motor learning under altered kinematic and dynamic environments. J. Neurosci. *19,* RC34 1–5.

Georgopoulos, A.P., Lurito, J.T., Petrides, M., Schwartz, A.B., and Massey, J.T. (1989). Mental rotation of the neuronal population vector. Science *243*, 234–236.

Giszter, S.F., Mussa-Ivaldi, F.A., and Bizzi, E. (1993). Convergent force fields organized in the frog's spinal cord. J. Neurosci. *13*, 467–491.

Gold, J.I., and Shadlen, M.N. (2000). Representation of a perceptual decision in developing oculomotor commands. Nature *404*, 390–394.

Graziano, M.S., Yap, G.S., and Gross, C.G. (1994). Coding of visual space by premotor neurons. Science *11*, 1054–1057.

He, S.Q., Dum, R.P., and Strick, P.L. (1993). Topographic organization of corticospinal projections from the frontal lobe: motor areas on the lateral surface of the hemisphere. J. Neurosci. *13*, 952–980.

He, S.Q., Dum, R.P., and Strick, P.L. (1995). Topographic organization of corticospinal projections from the frontal lobe: motor areas on the medial surface of the hemisphere. J. Neurosci. *15*, 3284–3306.

Hepp-Reymond, M.C., Husler, E.J., Maier, M.A., and Qi, H.X. (1994). Force-related neuronal activity in two regions of the primate ventral premotor cortex. Can. J. Physiol. Pharmacol. *72*, 571–579.

Hernandez, A., Zainos, A., and Romo, R. (2002). Temporal evolution of a decision-making process in medial premotor cortex. Neuron *33*, 959–972.

Hikosaka, O., Sakai, K., Nakahara, H., Lu, S., Miyachi, S., Nakamura, K., and Rand, M.K. (2000). The New Cognitive Neuroscience (Cambridge, MA: MIT Press).

Imamizu, H., Miyauchi, S., Tamada, T., Sasaki, Y., Takino, R., Putz, B., Yoshioka, T., and Kawato, M. (2000). Human cerebellar activity reflecting an acquired internal model of a new tool. Nature *13*, 192–195.

Johnson, M.T.V., Coltz, J.D., Hagen, M.C., and Ebner, T.J. (1999). Visuomotor processing as reflected in the directional discharge of premotor and primary motor cortex neurons. J. Neurophysiol. *81*, 875–894.

Kalaska, J.F., and Crammond, D.J. (1992). Cerebral cortical mechanisms of reaching movements. Science *255*, 1517–1523.

Kalaska, J.F., Cohen, D.A.D., Hyde, M.L., and Prud'homme, M. (1989). A comparison of movement direction-related versus load direction-related activity in the primate motor cortex, using a two-dimensional reaching task. J. Neurosci. *9*, 2080–2102.

Kalaska, J.F., Cohen, D.A., Prud'homme, M., and Hyde, M.L. (1990). Parietal area 5 neuronal activity encodes movement kinematics, not movement dynamics. Exp. Brain Res. *80*, 351–364.

Kawato, M. (1999). Internal models for motor control and trajectory planning. Curr. Opin. Neurobiol. *9*, 718–727.

Krakauer, J.W., Ghilardi, M.F., and Ghez, C. (1999). Independent learning of internal models for kinematic and dynamic control of reaching. Nat. Neurosci. *2*, 1026–1031.

Kurata, K., and Wise, S.P. (1988). Premotor and supplementary motor cortex in rhesus monkeys: neuronal activity during externally-and internally-instructed motor tasks. Exp. Brain Res. *72*, 237–248.

Li, C.-S.R., Padoa-Schioppa, C., and Bizzi, E. (2001). Neural correlates of motor performance and motor learning in the primary motor cortex of monkeys adapting to an external force field. Neuron *30*, 593–607.

Luppino, G., Matelli, M., Camarda, R.M., Gallese, V., and Rizzolatti, G. (1991). Multiple representations of body movements in mesial area 6 and the adjacent cingulate cortex: an intracortical microstimulation study in the macaque monkey. J. Comp. Neurol. *311*, 463–482.

Matelli, M., Luppino, G., and Rizzolatti, G. (1991). Architecture of superior and mesial area 6 and the adjacent cingulate cortex in the macaque monkey. J. Comp. Neurol. *311*, 445–462.

Matsuzaka, Y., Aizawa, H., and Tanji, J. (1992). A motor area rostral to the supplementary motor area (presupplementary motor area) in the monkey: neuronal activity during a learned motor task. J. Neurophysiol. *68*, 653–662.

Mussa-Ivaldi, F.A., and Bizzi, E. (2000). Motor learning through the combination of primitives. Philos. Trans. R. Soc. Lond. B Biol. Sci. *355*, 1755–1769.

Mussa-Ivaldi, F.A., Giszter, S.F., and Bizzi, E. (1994). Linear combinations of primitives in vertebrate motor control. Proc. Natl. Acad. Sci. USA *91*, 7534–7538.

Neter, J., Wasserman, W., and Kutner, M.H. (1985). Applied Linear Statistical Models (Homewood, IL: R. Irwing, Inc.).

Newsome, W.T. (1997). The king solomon lectures in neuroethology. Deciding about motion: linking perception to action. J. Comp. Physiol. [A] *181*, 5–12.

Olson, C.R., and Gettner, S.N. (1995). Object-centered direction selectivity in the macaque supplementary eye field. Science *18*, 985–988.

Penfield, W., and Welch, K. (1951). The supplementary motor area of the cerebral cortex. Arch. Neurol. Psychiatry *66*, 289–317.

Picard, N., and Strick, P.L. (1996). Motor areas of the medial wall: a review of their location and functional activation. Cereb. Cortex *6*, 342–353.

Picard, N., and Strick, P.L. (2001). Imaging the premotor areas. Curr. Opin. Neurobiol. *11*, 663–672.

Prut, Y., and Fetz, E.E. (1999). Primate spinal interneurons show pre-movement instructed delay activity. Nature *401*, 590–594.

Riehle, A., and Requin, J. (1993). The predictive value for performance speed of preparatory changes in neuronal activity of the monkey motor and premotor cortex. Behav. Brain Res. *53*, 35–49.

Saltzman, E. (1979). Levels of sensorimotor representation. J. Math. Psychol. *20*, 91–163.

Shadmehr, R., and Holcomb, H.H. (1997). Neural correlates of motor memory consolidation. Science *277*, 821–825.

Shadmehr, R., and Mussa-Ivaldi, F.A. (1994). Adaptive representation of dynamics during learning of a motor task. J. Neurosci. *14*, 3208–3224.

Shen, L., and Alexander, G.E. (1997). Preferential representation of instructed target location versus limb trajectory in dorsal premotor area. J. Neurophysiol. *77*, 1195–1212.

Shidara, M., Kawano, K., Gomi, H., and Kawato, M. (1993). Inverse-dynamics model eye movement control by Purkinje cells in the cerebellum. Nature *365*, 50–52.

Shima, K., and Tanji, J. (2000). Neuronal activity in the supplementary and presupplementary motor areas for temporal organization of multiple movements. J. Neurophysiol. *84*, 2148–2160.

Tanji, J. (1994). The supplementary motor area in the cerebral cortex. Neurosci. Res. *19*, 251–268.

Tanji, J., Kurata, K., and Okano, K. (1985). The effect of cooling of the supplementary motor cortex and adjacent cortical areas. Exp. Brain Res. *60*, 423–426.

Thach, W.T. (1978). Correlation of neural discharge with pattern and force of muscular activity, joint position, and direction of intended next movement in motor cortex and cerebellum. J. Neurophysiol. *41*, 654–676.

Thaler, D., Chen, Y.C., Nixon, P.D., Stern, C.E., and Passingham, R.E. (1995). The functions of the medial premotor cortex. I. Simple learned movements. Exp. Brain Res. *102*, 445–460.

Thoroughman, K.A., and Shadmehr, R. (1999). Electromyographic correlates of learning an internal model of reaching movements. J. Neurosci. *19*, 8573–8588.

Werner, W., Bauswein, E., and Fromm, C. (1991). Static firing rates of premotor and primary motor cortical neurons associated with torque and joint position. Exp. Brain Res. *86*, 293–302.

Wise, S.P. (1996). Corticospinal efferents of the supplementary sensorimotor area in relation to the primary motor cortex. Adv. Neurol. *70*, 57–69.

Wise, S.P., di Pellegrino, G., and Boussaoud, D. (1992). Primate

premotor cortex: dissociation of visuomotor from sensory signals. J. Neurophysiol. *68*, 969–972.

Wise, S.P., Boussaoud, D., Johnson, P.B., and Caminiti, R. (1997). Premotor and parietal cortex: corticocortical connectivity and combinatorial computations. Annu. Rev. Neurosci. *20*, 25–42.

Wolpert, D.M., and Ghahramani, Z. (2000). Computational principles of movement neuroscience. Nat. Neurosci. *3*, 1212–1217.

Woolsey, C.N., Settlage, P.H., Meyer, D.R., Sencer, W., Pinto Hamuly, T., and Travis, A.M. (1952). Patterns of localization in precentral and "supplementary" motor areas and their relation to the concept of premotor area. Res. Publ. Assoc. Nerv. Ment. Dis. *30*, 231–250.